Rev. Roum. Sci. Techn.– Électrotechn. et Énerg.
Vol. **63**, *2*, pp. 132–137, Bucarest, 2018

Dedicated to the memory of Academician Andrei Țugulea

STATISTICAL APPROACH OF UNDERWATER MAGNETIC FIELD MEASUREMENTS OF THE NAVAL MAGNETIC SIGNATURE

GEORGIANA ROSU[1], GHEORGHE SAMOILESCU[2], OCTAVIAN BALTAG[3]

Keywords: Fluxgate, Magnetic field measurement, Magnetometer, Measurement uncertainty, Statistical analysis.

This paper describes a particularly manufactured measuring device for ship magnetic signature and presents a statistical analysis of the measured data. A novel method specific to this type of magnetic measurement is developed and applied to the available data. There are analyzed the sources of uncertainty that affect the measurement and there is developed a specific model for the assessment of the uncertainty in magnetic field measurements with fluxgate transducers. Based on the operating principle of the fluxgate magnetometer, there were identified the main sources of uncertainty and their impact on measurements was computed. Finally, the resulting magnetic signature is reported as a value range determined by the combined uncertainty.

1. INTRODUCTION

Accurate and periodic determination of the ship's magnetic signature is imposed by security issues [1–6], and for this purpose there are employed high resolution and low power magnetometers such as the fluxgate transducers [7, 8]. In this paper, there is described the fluxgate magnetometer used for underwater measurements of a ship's magnetic signature, and the obtained data is statistically processed, in order to detect outliers and systematic errors [9]. The assessment of uncertainty is required in the case of each measurement procedure. Usually, the assessment is based on the identification of determinative parameters, when a relationship is available [10–13]. This paper describes a method for assessing uncertainty for the specific application of underwater magnetic field measurements using fluxgate transducers. There are described the stages of the uncertainty estimation process, starting from the identification of the determinative quantities and factors which affect the measurement, in order to estimate their impact on the data.

2. MEASUREMENT DEVICE DESCRIPTION

The main element of the fluxgate transducer is the saturable core manufactured of a ferromagnetic material with high magnetic permeability (permalloy). The ferromagnetic core is subjected simultaneously to the action of two magnetic fields, which are a constant field that is measured, and an excitation, variable, of odd symmetry field. In the case of the simplest form of the fluxgate transducer, the ferromagnetic core is surrounded by two windings, for excitation and signal, as represented in Fig. 1 [6, 7]. The primary coil is the excitation one, through which the core is periodically saturated by an alternating current. In the signal coil is induced the output voltage, that contains the even order harmonics of the excitation current, among which the second harmonic renders information of the measured field's strength and polarity [6]. The fluxgate transducer employed in the measurements actually has two additional windings: a negative reaction winding and a compensation winding. Figure 2 illustrates the successive manufacturing stages of the fluxgate transducer.

The operating principle of the fluxgate transducer is graphically represented in Fig. 3 [7]. A simplified magnetization characteristic of the ferromagnetic core is illustrated in Fig. 3a. The magnetic field generated by the current, which flows through the excitation coil has an alternating variation, as represented in Fig. 3b, c with the continuous line.

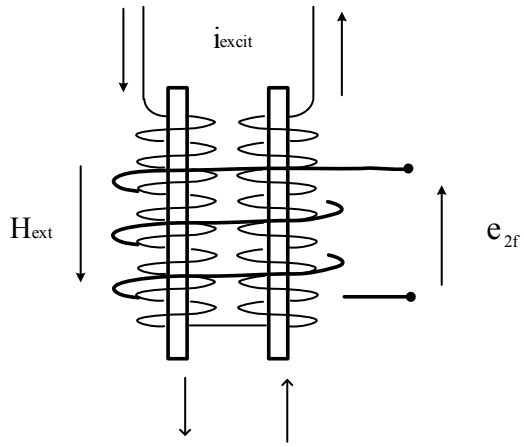

Fig. 1 – The schematic of the Vacquier-Forster fluxgate transducer with two parallel cores and two coils: excitation and measurement coil.

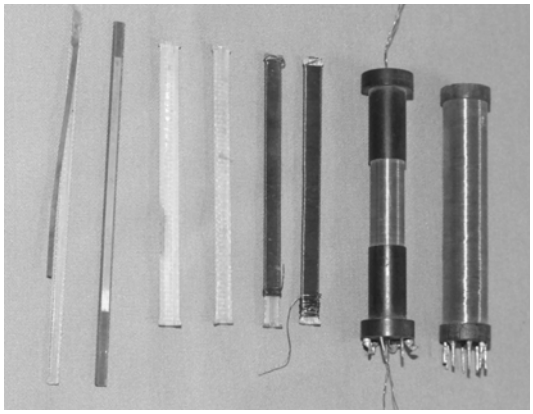

Fig. 2 – Stages of manufacturing the fluxgate transducer, with several windings, for: excitation, signal, negative feedback and compensation/calibration.

When there is a constant positive external field H_{ext}, an offset value is added, and the resulting field is represented with a dashed line. The ferromagnetic core magnetization is determined by the magnetization characteristic in Fig. 3a, and the excitation field H is presented in Fig. 3 b, c.

[1] Military Technical Academy, 39-49 George Cosbuc Blvd., Bucharest, georgianamarin01@gmail.com
[2] "Mircea cel Batran" Naval Academy, 1st Fulgerului Street, Constanta
[3] "Alexandru Ioan Cuza" University, Iasi, Faculty of Physics & "Terraflux Control LTD", Iasi

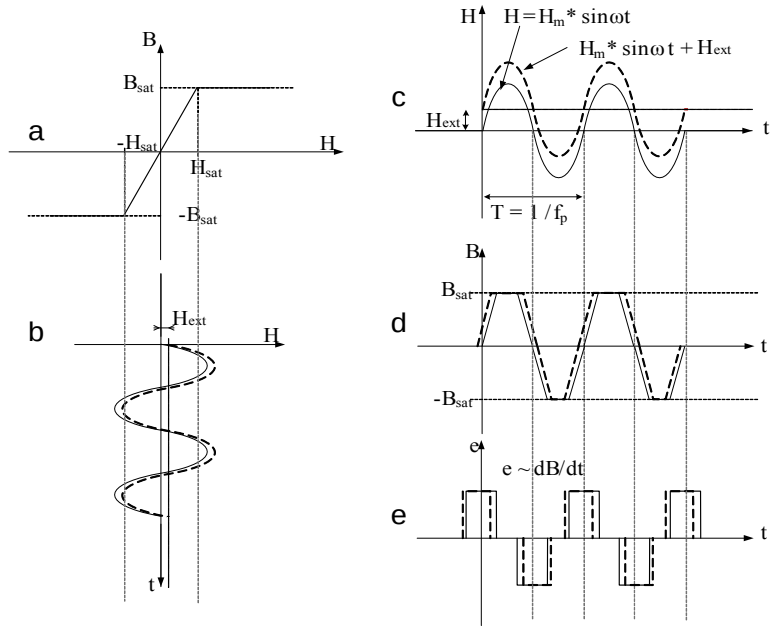

Fig. 3 – Operation principle of the fluxgate sensor: a) simplified magnetization characteristic of the core; b), c) excitation signal H with and without the external field h; d) the magnetic induction B within the core; e) the output induced voltage pulses e.

Without the external field H_{ext}, the magnetic flux density has a symmetrical trapezoidal shape, varying between its saturation limits $-B_{sat}$, $+B_{sat}$ with equal rising and falling edges. It is worth mentioning that the field denoted by H_{ext} represents the component of the external field that has the same direction as the ferromagnetic core and the measurement coil axis.

An induced voltage is thus generated at the signal coil, resulting in a series of symmetric alternating positive and negative pulses, represented with continuous line. Since the output signal in the absence of an external field is composed of symmetric alternating rectangular pulses, it lacks the even order harmonics.

For an external field, the quantities are represented with a dashed line, hence: the magnetic induction variation is no longer symmetrical – the falling edge is delayed, whereas the rising edge is phased ahead. Thus, there is obtained an unsymmetrical induced voltage, from which the second harmonic is extracted, having the following expression [7]:

$$e(2\omega t) = -10^{-8} N_S \quad A \quad 8\mu_{ef} f_p H_{ext} \frac{2H_{sat}}{H_{\max}} \cdot \sqrt{1-\left(\frac{H_{sat}}{H_{\max}}\right)^2} \sin(2\omega t). \tag{1}$$

The physical quantities involved in (1) are [7]:

- $e(2\omega t)$ – second order harmonic of the induced voltage;
- N_s – number of turns of the signal winding;
- A –transversal section of the ferromagnetic core;
- μ_{ef} – core's effective permeability, depending on the material's permeability and its dimensions;
- f_p – the excitation signal frequency;
- ω – angular frequency;
- H_{ext} – the measured field;
- H_{sat} – magnetic field intensity corresponding to the saturation induction B_{sat};
- $H_{\max}$ – the magnitude of the excitation field.

The numerical values derive from the linear approximation of the magnetization characteristic of the core.

The sensor's directionality needs to be taken into consideration, as well as the fact that the sensor's purpose is to measure the vertical component of the field H_Z, and that the sensor may not be perfectly aligned to the vertical component. Let φ denote the angle between the vertical magnetic field H_Z and the ferromagnetic core axis. By considering the above mentioned arguments and using as notation for the the fluxgate sensitivity the letter S [6], the expression in (1) is thus adapted:

$$e(2\omega t) = S \cdot H_Z \cdot \cos\varphi \,. \tag{2}$$

The fluxgate sensitivity S in (2) is obtained by including all terms in (1) except for the external field H_{ext}. In fact, H_Z represents the vertical component of the external field H_{ext}, which is meant to be measured.

The simplified electric diagram of the magnetometer is shown in Fig. 4. The signal generator applies a signal of frequency equal to 20 kHz ($4f_p$) to a divider providing a reference voltage of 10 kHz ($2f_p$) required for the command of the synchronous detector. The same divider supplies a 5 kHz (f_p) signal to a set of mono-flop circuits, which adjust the phase of the excitation signal. It generates two pulse trains delayed by 180°, amplified and transmitted by the excitation winding.

The excitation signal required by the fluxgate magnetometer has the frequency f_p = 5 kHz and consists of pulses with an amplitude of ± 10 V. The second harmonic signal is 10 times amplified and transmitted to the synchronous detector providing the detection of the 10 kHz ($2f_p$) reference signal. The signal is then filtered; the resultant voltage magnitude is proportional to the external field, which is further sent to an analog-digital converter, for display. The same dc voltage is amplified and applied to the negative feedback winding. A voltage-controlled current source is used for ambient field compensation. Calibration is obtained by changing the feedback current.

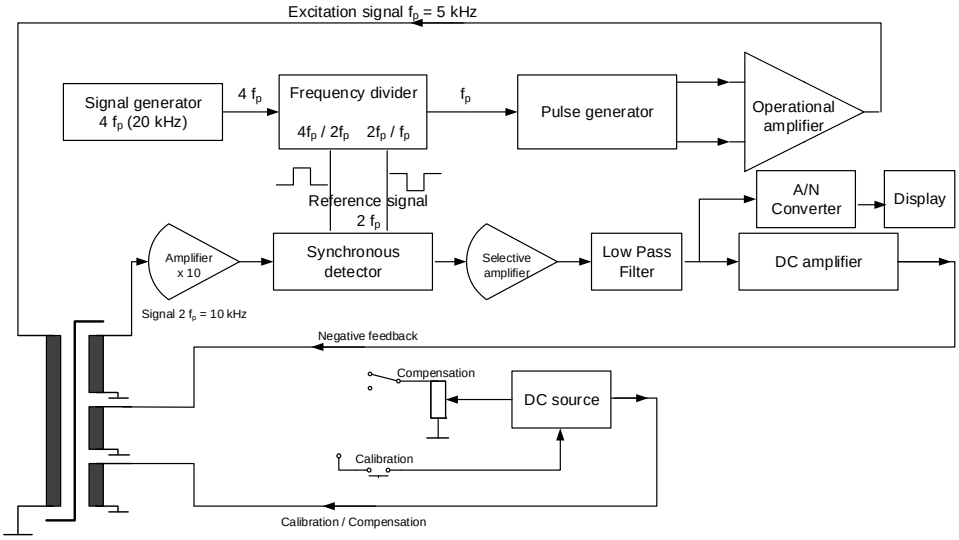

Fig. 4 – Simplified electrical diagram of the fluxgate magnetometer employed in measurements.

3. MEASUREMENT SETUP AND RESULTS

The equipment employed in the underwater magnetic measurements is composed of three fluxgate sensors and a three-channel magnetometer, manufactured by "Terraflux Control LTD", Iasi. The magnetometer is designed to measure the vertical component of the ship magnetic field strength, due to the measurement set-up assembly. The device is designed to indicate the magnetic field strength in CGS units (mOe). The measurement range is ±64 A/m (±800 mOe), and the maximum sensor depth is 40 meters.

Three field transducers are mounted on a supporting beam placed in the ship's transversal plane, and are moved along the ship, from bow to stern. The beam is made of aluminum and is 5.5 meters in length. The transducers were placed as it follows: one in the center, below the ship keel, and the other two in the board sides at 2.7 m distance from the center one. The measurement set-up is described in Fig. 5. The vertical component of the ship magnetic field is measured along the ship at a depth of 7 meters below the keel. For each measurement point there were taken a set of approximately 100 values within a range of 30–35 seconds for each of the three transducers. There have been found time variations for each measuring point and for each sensor. The recorded values include the Earth's magnetic field [14–16]. Thus, there we obtained 46 measurement points, with three sets of data for each point, corresponding to the three sensors. The measured data for a single position of the transversal grid is illustrated in Fig. 6. Due to large variations of the resulting signal, there is imposed the statistical processing of the measured data [9].

4. STATISTICAL ANALYSIS OF MEASURED DATA

Interpretation of the measurement results was made based on application of validity, randomness, and compliance tests [9]. Validity tests serve for identification of error, which affects the results that deviate in a significant amount from the average value. In the first stage of processing measurement data, the Chauvenet test was applied [9]. According to Chauvenet's criterion, an outlier is any value whose probability of emergence is lower than a threshold, which is determined by the sample size n – the total number of measured values. Thus, there is obtained an interval of data around the mean value, and any value located outside this interval is an outlier [9]. If the Chauvenet criterion is applied successively, it can yield a significant amount of outliers, which would decrease the sample size and the power of the statistical test.

Therefore, the Chauvenet validity test results were confronted with the outlier analysis using Tukey's boxplot method [10] with the IBM SPSS (Statistical Package for the Social Sciences) software [11]. SPSS is a software tool used for statistical analysis; it was initially designed for social studies, but it is currently employed in several fields, including medical research, market research, and measurement data processing [11]. Tukey's boxplot method is a graphical tool meant to identify outliers, by comparing the extreme values with the lower and upper limits of an interval computed based on the first and third quartiles of the data set.

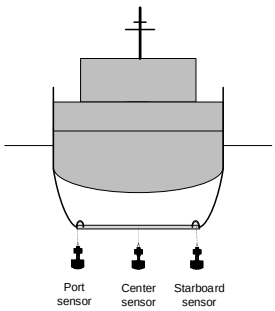

Fig. 5 – Measurement set-up of the three fluxgate transducers placed below the ship, in a transversal plane, and moved along the ship.

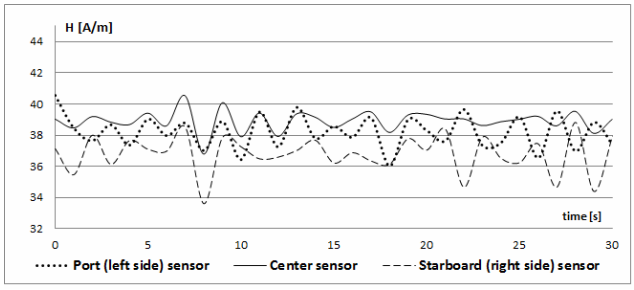

Fig. 6 – Time variations of magnetic field measured by the three sensors – port, center, and starboard.

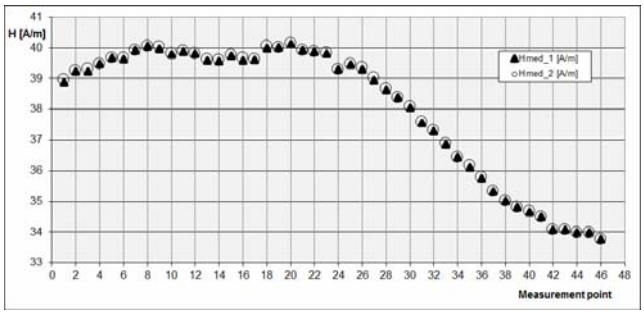

Fig. 7 – The average value of magnetic field intensity before (H_{med_1}) and after (H_{med_2}) outlier rejection.

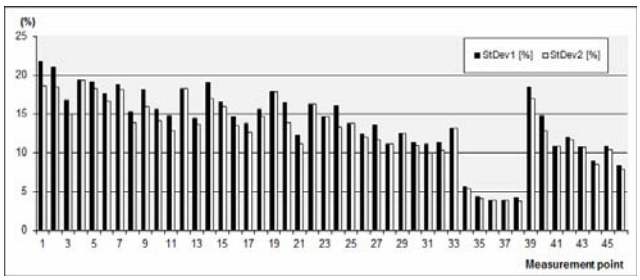

Fig. 8 – The standard deviation of magnetic field values before (StDev_1) and after (StDev_2) outlier rejection.

After the outlier data analysis, there were rejected 206 values for all the measurement points. The effect of outliers' rejection restricts the variation range for the analyzed variables, which are the magnetic field values recorded by the three sensors: positioned near port, below the ship keel and near starboard. Figures 7 and 8 illustrate the average value and standard deviation of the data set measured by the center sensor located below the keel, before and after the outlier rejection.

After removing outliers, the Young test [12] is used in order to test the data randomness. The Young test reveals the existence of systematic errors. These can be given by the Earth's magnetic field, which is included in the measured values of the ship magnetic field. However, it is necessary to assess the measurement uncertainty.

5. DETERMINATION OF THE MEASUREMENT UNCERTAINTY

In order to analyze the relevant sources of uncertainty, there are identified their effects on the measurement result in a cause-effect diagram (Ishikawa diagram) – illustrated in Fig. 9 [12, 13]. The chart axis is the measured quantity – the magnetic field strength's vertical component H_Z, whereas the main branches represent the input parameters: fluxgate sensitivity, angle of orientation and output voltage, and the display of the analog-digital converted signal. For each main branch there are added factors that can affect the main parameters. Apart from these main sources of uncertainty, there may be other sources of error, arising from: imperfect definition of the measured quantity, insufficient knowledge of environmental conditions, and the alteration of measuring devices quality parameters due to voltage and frequency variations in the onboard electrical network. Based on the general expression for the output voltage in (2), the measured field H_Z is dependent on the magnetometer sensitivity S (assumed constant), the output voltage U and the tilt angle φ between the magnetic field vector and the sensor axis:

$$H_Z = \frac{U}{S \cdot \cos\varphi}. \tag{3}$$

In order to quantify the uncertainty associated with the resulting variable, the uncertainty of each source is assessed and the combined uncertainty is then calculated. The general relationship between the standard uncertainty of the measured quantity $u_c(y)$ and standard uncertainties $u(x_i)$ of the independent variables $x_1, x_2, \ldots, x_n$ is [12]:

$$u_c\left(y(x_1, x_2, \ldots, x_n)\right) = \sqrt{\sum_{i=1}^{n} {c_i}^2 \, u(x_i)^2}\ . \tag{4}$$

Here c_i are called sensitivity coefficients and they assess the partial derivative of y to x_i. Considering the particular case of magnetic field measurement with fluxgate sensor, (4) is adapted to take into account the following uncertainty sources: the signal coil output voltage U and the angle φ

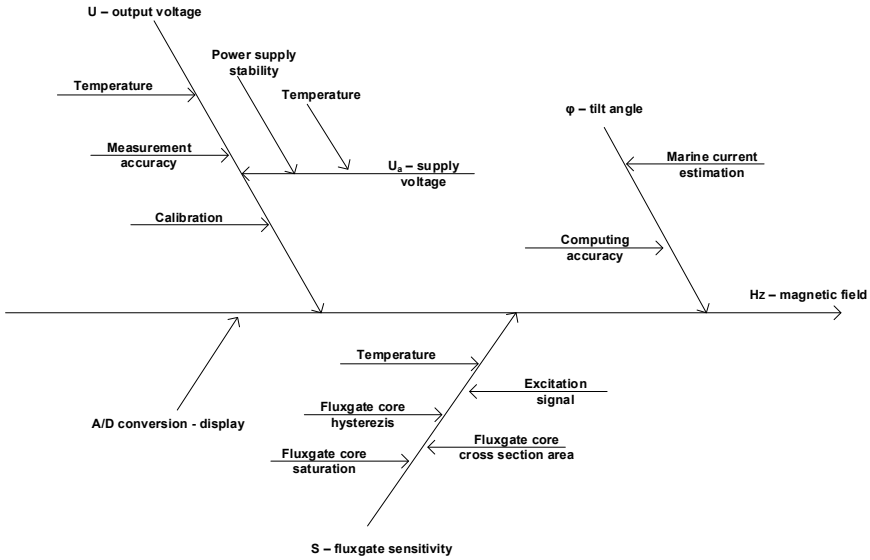

Fig. 9 – Cause-effect diagram for magnetic field measurement with fluxgate magnetometer.

between the fluxgate axis and the field vector, whereas the fluxgate sensitivity *S* is considered constant. By differentiating (3) and replacing the sensitivity coefficients, it results:

$$\mathrm{d}H_Z = \frac{1}{S}\sec\varphi\cdot\mathrm{d}U + \frac{U}{S}\mathrm{tg}\varphi\sec\varphi\cdot\mathrm{d}\varphi. \qquad (5)$$

Considering that dH_Z, dU, and dφ are random errors of the respective quantities, these differentials can be expressed as the difference between individual values and their mean value. The relationship is then squared, summed up for the *n* individual values and then divided by *n* in order to get the average. For simplification, the average product of the differentials dU and dφ is considered null. Thus there is obtained the relationship between the standard uncertainty of the measured quantity and the input quantities in (6). All quantities accentuated by an upper line $\overline{U}$, $\overline{\varphi}$, represent the average values of the respective quantities in the measurement set

$$u^2(H_Z) = \left(\frac{\sec\overline{\varphi}}{S}\right)^2\cdot u^2(U) + \left(\frac{\overline{U}\,\mathrm{tg}\overline{\varphi}\sec\overline{\varphi}}{S}\right)^2\cdot u^2(\varphi). \qquad (6)$$

To these sources of uncertainty determined by the independent parameters in the measured quantity formula, there are added sources illustrated as main branches in the cause-effect diagram. Therefore, the uncertainty budget consists of:

- uncertainty of the output voltage *u(U)*,
- uncertainty of the magnetometer sensitivity *u(S)*,
- uncertainty of the angle between the field vector and fluxgate axis *u(φ)*,
- uncertainty determined by the number of digits when displaying the field value *u(display)*, and
- the uncertainty of determining the average value for each measurement point *u(* $\overline{H}_Z$ *)*.

Each of the uncertainties is assessed based on the distribution type of the respective variable.

For the output voltage there was performed a set of observations on the parameter variation. Due to the random variation, there was determined a normal distribution (type A) of average value 0 V and standard deviation s = 0.1 V.

For the angle φ parameter, there is estimated a maximum variation range $\varphi \pm a$, described by a symmetrical triangular distribution, because the values that are closer to the average value have a higher probability than the marginal values. The average value of the angle is equal the declination of the Earth's magnetic field in the measurement area – approximately 60°, based on the IGRF (International Geomagnetic Reference Field) model [16].

By composing the forces acting upon the transducer – the marine current in the measurement area [17] and the transducer weight – there yields a maximum tilt angle of the transducer of 3°, resulting in the angle uncertainty of $u(\varphi)$ = 1.2247°. The uncertainty associated with the display of the magnetic field value is described by a rectangular distribution of width equal to 0.0039 A/m (0.05 mOe), which is the display accuracy. The uncertainty in determining the field's average value *u(* $\overline{H}_Z$ *)* in each measurement point is computed by the ratio between the standard deviation *s* and the square root of the total number of values *n*.

In order to report an accurate measurement result, the combined uncertainty must be computed, based on the uncertainty budget, listed in Table 1. The vertical magnetic signature appears as a value range, consisting of the mean value $H_{Zmed} \pm u_c(H_Z)$ the combined uncertainty calculated at each point of measurement.

Figure 10 illustrates the vertical component of magnetic field recorded in the corresponding ship area, by the center sensor below the ship keel, including the Earth's magnetic field. The range of values shown in green is centered on the mean field value H_{Zmed} at the measurement point.

The combined uncertainty is approximately 11 %, in most measurement points. From the analysis of the uncertainty budget, there emerges the major influence of the signal winding output voltage uncertainty due to the high value of the sensitivity coefficient.

Table 1

The uncertainty budget

Source	**Distribution type**	**Standard uncertainty**		**Sensitivity coefficient**	
		Formula	**Value**	**Formula**	**Value**
Output voltage	Type A / normal	$u(U) = s$	0.1 V	$\frac{\partial H_Z}{\partial U} = \frac{\sec\overline{\varphi}}{S}$	4.95 (A/m/) V
Angle between the magnetic field and fluxgate axis	Type B / triangular	$u(\varphi) = \frac{\varphi_{\max}}{\sqrt{6}}$	1.2247 °	0.59	7.42 (A/m)/°
Fluxgate sensitivity	Type B / rectangular	$u(S) = \frac{S_{\max}}{\sqrt{3}}$	0.0175 V/(A/m)	-	1 (A/m)/ V
Field value display	Type B / rectangular	$u(display) = \frac{0.05}{\sqrt{3}}$	0.0023 A/m	-	1
Field average value	Type A / normal	$u(\overline{H}_Z) = \frac{s}{\sqrt{n}}$	computed in each of the n points (A/m)	-	1
Combined uncertainty	$u_C(H_Z) = \sqrt{\left(\frac{\sec\overline{\varphi}}{S}\right)^2\cdot u^2(U) + \left(\frac{\overline{U}\,\mathrm{tg}\overline{\varphi}\sec\overline{\varphi}}{S}\right)^2\cdot u^2(\varphi) + u^2(S) + u^2(display) + u^2(\overline{H}_Z)}$				

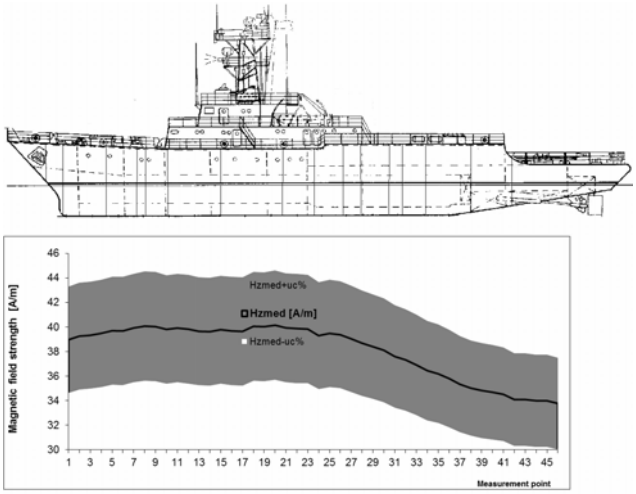

Fig. 10 – Vertical magnetic signature measured along the ship with center sensor, in the indicated range of combined uncertainty.

6. CONCLUSIONS

The paper describes a particular type of sensor used in underwater measurements of the ship's magnetic field – the vertical component, which is the most significant in actuating magnetic mines lying on the seabed. Since the ship's magnetism is determined not only by properties of the ferromagnetic material [18–20] used in the ship's hull and equipment [2], but also on the ship's main dimensions and the geomagnetic field acting upon it [4], the most accurate determination of the ship's magnetic signature is obtained through *in situ* measurements. There has been developed a novel, specific model for assessing uncertainty in measuring the ship magnetic field with fluxgate transducers. This took into account the influence of the input parameters: fluxgate sensitivity, inclination between the fluxgate axis and the field vector, the output voltage, the display signal received from the analog-digital converter. Based on the estimation model, the budget of uncertainty was computed, resulting in the combined uncertainty about ±11 % in most measurement points. The uncertainty budget highlights the major impact of the signal winding output voltage uncertainty due to the high value of its sensitivity coefficient. The fluxgate output voltage was most likely affected by variations in voltage and frequency of the ship's power network.

Received on March 16, 2018

REFERENCES

1. G. Aird, *Modelling the Induced Magnetic Signature of Naval Vessels*, University of Glasgow, Glasgow, 2000, pp. 14–45.
2. J. Holmes, *Modeling a Ship's Ferromagnetic Signatures*, Morgan & Claypool, 2007, pp. 17–45.
3. G. Marin, G. Samoilescu, O. Baltag, D. Costandache, I. Rau, *The Analysis of Model Accuracy and Magnetic Signature of a Ship Scale Model*, Rev. Roum. Sci. Techn. – Électrotechn. et Énerg., **59**, *3*, pp. 269–278 (2014).
4. G. Rosu, *Development, Analysis and Exploitation of Naval Magnetic Signature Models* (in Romanian), Performantica Publishing House, Iasi, 2015, pp. 125–147.
5. G. Samoilescu, G. Marin, *Ship's magnetic field characteristics in normal depth plane*, Land Forces Academy Scientific Bulletin, **15**, *1*, pp. 80-84 (2010).
6. O. Baltag, D. Costandache, O Robu., V. Ignat, *Magnetometry* (in Romanian), Inventica Publishing House, Iasi, 2001, pp. 153–167.
7. W.A. Geyger, *Nonlinear magnetic devices*, Ed. Tehnica, 1968.
8. S. Tumanski, *Handbook of Magnetic Measurements*, CRC Press, 2011, pp. 351–354.
9. P.H. Menold, R.K. Pearson, F. Allgower, *Online Outlier Detection and Removal*, Proceedings of the 7th Mediterranean Conference on Control and Automation, Haifa (Israel), June 28–30, 1999.
10. B. M. Ayyub, G. J Klir, Uncertainty Modeling and Analysis in Engineering and the Sciences, Chapman & Hall/CRC, 2006, pp. 321–340.
11. IBM SPSS, available at: www.ibm.com/analytics/data-science/predictive-analytics/spss-statistical-software.
12. S.L.R. Ellison, M. Rosslein, A. Williams (Editors), *Eurachem/Citac Guide, Quantifying uncertainty in analytical measurement*, Eurachem, 2000, pp. 16–32.
13. P. Fornasini, The Uncertainty in Physical Measurements. An Introduction to Data Analysis in the Physics Laboratory, Springer, 2008, pp. 155–168.
14. R. Lanza, A. Meloni, The Earth's Magnetism. An Introduction for the Geologists, Springer, 2006, pp. 59–67.
15. A. Tugulea, I.V. Nemoianu, *Quasi-stationary electrokinetic models of Earth's magnetic internal field sources*, Rev. Roum. Sci. Techn. – Électrotechn. et Énerg., **56**, *2*, pp. 149–159 (2011).
16. International Geomagnetic Reference Field, available at: http://www.ngdc.noaa.gov/IAGA/vmod/igrf.html.
17. Y.P. Neprochnov, P.P. Shirshov, D.A. Ross, *Black Sea geophysical framework (Deep Sea Drilling Project)*, **XLII**, *2*, pp. 1043-1055 (2007).
18. V. Ionita, L. Petrescu, *Magnetic material characterization by open sample measurements*, Rev. Roum. Sci. Techn. – Électrotechn. et Énerg., **54**, *1*, pp. 87–94 (2009).
19. P.C. Andrei, M. Maricaru, S. Marinescu, M. Stanculescu, I.F. Hantila, *An efficient procedure to assess the static magnetization relationship*, Rev. Roum. Sci. Techn. – Électrotechn. et Énerg., **61**, *2*, pp. 101–105 (2016).
20. V. Ionita, L. Petrescu, E. Cazacu, *Effect of current harmonics on the hysteresis losses in soft magnetic materials*, Rev. Roum. Sci. Techn. – Électrotechn. et Énerg., **60**, *4*, pp. 366–375 (2015).